

Effective Edge-wise Representation Learning in Edge-Attributed Bipartite Graphs

Hewen Wang
National University of Singapore
Singapore, Singapore
wanghewen@u.nus.edu

Renchi Yang
Hong Kong Baptist University
Hong Kong SAR, China
renchi@hkbu.edu.hk

Xiaokui Xiao
National University of Singapore
Singapore, Singapore
xkxiao@nus.edu.sg

ABSTRACT

Graph representation learning (GRL) is to encode graph elements into informative vector representations, which can be used in downstream tasks for analyzing graph-structured data and has seen extensive applications in various domains. However, the majority of extant studies on GRL are geared towards generating node representations, which cannot be readily employed to perform edge-based analytics tasks in *edge-attributed bipartite graphs* (EABGs) that pervade the real world, e.g., spam review detection in customer-product reviews and identifying fraudulent transactions in user-merchant networks. Compared to node-wise GRL, learning edge representations (ERL) on such graphs is challenging due to the need to incorporate the structure and attribute semantics from the perspective of edges while considering the separate influence of two heterogeneous node sets \mathcal{U} and \mathcal{V} in bipartite graphs. To our knowledge, despite its importance, limited research has been devoted to this frontier, and existing workarounds all suffer from sub-par results.

Motivated by this, this paper designs EAGLE, an effective ERL method for EABGs. Building on an in-depth and rigorous theoretical analysis, we propose the *factorized feature propagation* (FFP) scheme for edge representations with adequate incorporation of long-range dependencies of edges/features without incurring tremendous computation overheads. We further ameliorate FFP as a dual-view FFP by taking into account the influences from nodes in \mathcal{U} and \mathcal{V} severally in ERL. Extensive experiments on 5 real datasets showcase the effectiveness of the proposed EAGLE models in semi-supervised edge classification tasks. In particular, EAGLE can attain a considerable gain of at most 38.11% in AP and 1.86% in AUC when compared to the best baselines.

CCS CONCEPTS

• **Computing methodologies** → **Supervised learning by classification**; **Factorization methods**; • **Mathematics of computing** → **Graph algorithms**.

KEYWORDS

graph representation learning, edge classification, attributed graph, bipartite graph

ACM Reference Format:

Hewen Wang, Renchi Yang, and Xiaokui Xiao. 2024. Effective Edge-wise Representation Learning in Edge-Attributed Bipartite Graphs. In *Proceedings of the 30th ACM SIGKDD Conference on Knowledge Discovery and Data Mining (KDD '24)*, August 25–29, 2024, Barcelona, Spain. ACM, New York, NY, USA, 11 pages. <https://doi.org/10.1145/3637528.3671805>

1 INTRODUCTION

Edge-attributed bipartite graphs (EABGs) (a.k.a. attributed interaction graphs [62]) are an expressive data structure used to model the interactive behaviors between two sets of objects \mathcal{U} and \mathcal{V} where the behaviors are characterized by rich attributes. Practical examples of EABGs include reviews from users/reviewers on movies, businesses, products, and papers; transactions between users and merchants; and disease-protein associations.

In real life, EABGs have seen widespread use in detecting spam reviews in e-commerce [60], malicious incidents in telecommunication networks [52], fraudulent transactions/accounts in finance [44] or E-payment systems [25], abusive behaviors in online retail websites [41], insider threats from audit events [7], and others [5, 48]. The majority of such applications can be framed as edge-based prediction or classification tasks in EABGs.

In recent years, graph representation learning (e.g., graph neural networks and network embedding) has emerged as a popular and powerful technique for graph analytics and has seen fruitful success in various domains [14]. In a nutshell, GRL seeks to map graph elements in the input graph into feature representations (a.k.a. embeddings), based on which we can perform downstream prediction or classification tasks. However, to our knowledge, most of the existing GRL models, e.g., GCN [21], GraphSAGE [13] and GAT [39], are devised for learning node-wise representations in node-attributed graphs, and *edge-wise representation learning* (ERL), especially on EABGs, is as of yet under-explored. A common treatment for obtaining edge representations is to directly apply the canonical node-wise GRL models [3, 13, 17, 21, 39, 40, 46] to generate node embeddings, followed by concatenating them as the embeddings of the corresponding edges. Despite its simplicity, this methodology falls short of not only the accurate preservation of the graph topology from the perspective of edges (demanding an effective combination of node embeddings) but also the incorporation of the edge attributes in EABGs, thereby resulting in compromised embedding quality. Another category of workarounds is to simply transform the original EABGs into node-attributed unipartite graphs by converting the edges into nodes and connecting them if they share common endpoints in the input EABGs. In doing so, the node-wise GRL techniques can be naturally adopted on such projected graphs for deriving edge representations. Unfortunately, aside from information loss of the bipartite structure in the input EABG \mathcal{G} by the

Permission to make digital or hard copies of all or part of this work for personal or classroom use is granted without fee provided that copies are not made or distributed for profit or commercial advantage and that copies bear this notice and the full citation on the first page. Copyrights for third-party components of this work must be honored. For all other uses, contact the owner/author(s).
KDD '24, August 25–29, 2024, Barcelona, Spain
© 2024 Copyright held by the owner/author(s).
ACM ISBN 979-8-4007-0490-1/24/08
<https://doi.org/10.1145/3637528.3671805>

simple transformation [55, 64], such projection-based approaches rely on constructing an edge-to-edge graph \mathcal{G}' , which often entail immense space consumption (up to $O(m^2)$ in the worst case) due to the scale-free property of real-world graph \mathcal{G} , i.e., a few nodes connecting to a significant amount of nodes in \mathcal{G} and creating a multitude of edge-to-edge associations in \mathcal{G}' [54]. Recently, several efforts [2, 6, 19, 42] have been specifically invested towards learning edge-wise feature representations. However, these ERL models are either designed for unipartite graphs or hypergraphs and hence, cannot readily be applied to EABGs for high-quality representations, as they are unable to capture the unique characteristics of bipartite graphs, particularly the underlying semantics of connections to nodes in \mathcal{U} and \mathcal{V} from two heterogeneous sources.

To remedy the deficiencies of existing works, this paper presents EAGLE (Edge-wise BipArtite Graph Representation LEarning) for effective ERL in EABGs. By taking inspiration from the numeric analysis [27, 53, 66] of the most popular GRL solutions, i.e., classic message-passing (a.k.a. feature-propagation) GNNs, we begin by formalizing the edge-wise representation learning objective as an optimization problem, while considering the respective influence of edge associations with two sets of heterogeneous nodes \mathcal{U} and \mathcal{V} . Through our theoretical insights into the optimal solution to the optimization problem, the derived feature propagation rules, and their connections to the well-established Markov chain theory, we unveil the necessity of preserving long-range dependencies [49] of edges in edge representations on EABGs. Based thereon, we propose a *factorized feature propagation* (FFP) scheme to enable efficient and effective long-range feature propagation for generating edge representations in EAGLE. Furthermore, we upgrade EAGLE with the *dual-view factorized feature propagation* (DV-FFP) for flexible and full exploitation of semantics from two sets of nodes \mathcal{U} and \mathcal{V} in EABGs. More precisely, instead of combining edge associations to \mathcal{U} and \mathcal{V} via a given hyperparameter for subsequent ERL, DV-FFP learns two sets of edge embeddings using the connections to \mathcal{U} and \mathcal{V} , respectively, followed by an aggregator function that combines them as the final representations. Following previous work, our EAGLE models are trained by feeding the final edge representations into the loss function for the semi-supervised edge classification.

We evaluate the proposed EAGLE models against 9 baselines on 5 real EABGs in terms of semi-supervised edge classification tasks. The experimental results exhibit that our EAGLE models consistently achieve the best empirical performance over 5 datasets with remarkable gains, further validating the effectiveness of FFP and DV-FFP schemes in EAGLE. Notably, on the academic graphs AMiner and OAG dataset, EAGLE can obtain 38.11% and 11.97% performance gains in terms of average precision (AP) over the best competitor, indicating the superiority of EAGLE in learning predictive edge representations on EABGs.

The remainder of this paper is structured as follows. After presenting the preliminaries and formal problem definition in Section 2, we design the basic EAGLE model with FFP in Section 3. We further introduce an enhanced EAGLE model with dual-view FFP in Sections 4. Experiments are conducted in Section 5. Section 6 reviews related studies, and Section 7 concludes the paper.

2 PRELIMINARIES

Throughout this paper, sets are denoted by calligraphic letters, e.g., \mathcal{V} , and $|\mathcal{V}|$ is used to denote the cardinality of the set \mathcal{V} . Matrices (resp. vectors) are written in bold uppercase (resp. lowercase) letters, e.g., \mathbf{M} (resp. \mathbf{x}). The superscript \mathbf{M}^\top is used to symbolize the transpose of matrix \mathbf{M} . $\mathbf{M}[i]$ ($\mathbf{M}[:, i]$) is used to represent the i -th row (resp. column) of matrix \mathbf{M} . Accordingly, $\mathbf{M}[i, j]$ denotes the (i, j) -th entry in matrix \mathbf{M} . For each vector $\mathbf{M}[i]$, we use $\|\mathbf{M}[i]\|$ to represent its L_2 norm, i.e., $\|\mathbf{M}[i]\| = \sqrt{\sum_{j=1}^d \mathbf{M}[i, j]^2}$ and $\|\mathbf{M}\|_F$ to represent the Frobenius norm of \mathbf{M} , i.e., $\|\mathbf{M}\|_F = \sqrt{\sum_{i=1}^n \sum_{j=1}^d \mathbf{M}[i, j]^2}$.

2.1 Edge-Attributed Bipartite Graphs

Definition 2.1 (Edge-Attributed Bipartite Graphs (EABG)). An EABG is defined as $\mathcal{G} = (\mathcal{U} \cup \mathcal{V}, \mathcal{E}, \mathbf{X})$, where \mathcal{U} and \mathcal{V} represent two disjoint node sets, \mathcal{E} consists of the inter-set edges connecting nodes in \mathcal{U} and \mathcal{V} , and each edge e_i is associated with a length- d attribute vector $\mathbf{X}[i]$.

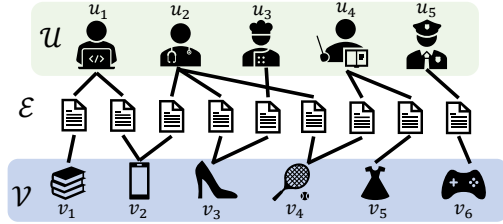


Figure 1: An Example EABG

Figure 1 exemplifies an EABG \mathcal{G} in online retail platforms (e.g., Amazon and eBay) with 5 users u_1 - u_5 in \mathcal{U} , 6 products v_1 - v_6 in \mathcal{V} , and the user-product interactions in \mathcal{E} . Each interaction (i.e., edge) is associated with a review (i.e., edge attributes) from the user on the product.

For each node $u_i \in \mathcal{U}$ (resp. $v_j \in \mathcal{V}$), \mathcal{E}_{u_i} (resp. \mathcal{E}_{v_j}) symbolizes the set of edges incident to u_i (resp. v_j). We use $\mathbf{D}_{\mathcal{U}} \in \mathbb{R}^{|\mathcal{U}| \times |\mathcal{U}|}$ (resp. $\mathbf{D}_{\mathcal{V}} \in \mathbb{R}^{|\mathcal{V}| \times |\mathcal{V}|}$) to represent the diagonal matrix whose diagonal entries correspond to the degrees of nodes in \mathcal{U} (resp. \mathcal{V}), e.g., $\mathbf{D}_{\mathcal{U}}[u_i, u_i] = |\mathcal{E}_{u_i}|$ and $\mathbf{D}_{\mathcal{V}}[v_i, v_i] = |\mathcal{E}_{v_i}|$. Then, $\mathbf{D} = \begin{pmatrix} \mathbf{D}_{\mathcal{U}} & 0 \\ 0 & \mathbf{D}_{\mathcal{V}} \end{pmatrix} \in \mathbb{R}^{(|\mathcal{U}|+|\mathcal{V}|) \times (|\mathcal{U}|+|\mathcal{V}|)}$ is the diagonal node degree matrix of \mathcal{G} . Further, we denote by $\mathbf{E}_{\mathcal{U}} \in \mathbb{R}^{|\mathcal{E}| \times |\mathcal{U}|}$ and $\mathbf{E}_{\mathcal{V}} \in \mathbb{R}^{|\mathcal{E}| \times |\mathcal{V}|}$ the edge-node indicator matrices for node sets \mathcal{U} and \mathcal{V} , respectively. More precisely, for each edge $e_i \in \mathcal{E}$ and its two end points $u^{(i)}, v^{(i)}$, we have $\mathbf{E}_{\mathcal{U}}[e_i, u^{(i)}] = \mathbf{E}_{\mathcal{V}}[e_i, v^{(i)}] = 1$. For other nodes $u \in \mathcal{U} \setminus u^{(i)}$ and $v \in \mathcal{V} \setminus v^{(i)}$, $\mathbf{E}_{\mathcal{U}}[e_i, u] = \mathbf{E}_{\mathcal{V}}[e_i, v] = 0$.

On the basis of $\mathbf{D}_{\mathcal{U}}$, $\mathbf{E}_{\mathcal{U}}$ and $\mathbf{D}_{\mathcal{V}}$, $\mathbf{E}_{\mathcal{V}}$, we define edge-wise transition matrix $\mathbf{P}_{\mathcal{U}}$ and $\mathbf{P}_{\mathcal{V}}$ as follows:

$$\mathbf{P}_{\mathcal{U}} = \mathbf{E}_{\mathcal{U}} \mathbf{D}_{\mathcal{U}}^{-1} \mathbf{E}_{\mathcal{U}}^\top \text{ and } \mathbf{P}_{\mathcal{V}} = \mathbf{E}_{\mathcal{V}} \mathbf{D}_{\mathcal{V}}^{-1} \mathbf{E}_{\mathcal{V}}^\top. \quad (1)$$

Lemma 2.2 unveils a unique property of $\mathbf{P}_{\mathcal{U}}$ and $\mathbf{P}_{\mathcal{V}}$, which is crucial to the design of our EAGLE model.

LEMMA 2.2. $\mathbf{P}_{\mathcal{U}}$ and $\mathbf{P}_{\mathcal{V}}$ are doubly stochastic matrices.

2.2 Problem Formulation

We formalize the *edge representation learning* (ERL) in EABGs as follows. Given an EABG $\mathcal{G} = (\mathcal{U} \cup \mathcal{V}, \mathcal{E}, \mathbf{X})$, the task of ERL aims to build a model $f : \mathcal{E} \rightarrow \mathbf{Z} \in \mathbb{R}^{|\mathcal{E}| \times z}$ ($z \ll |\mathcal{E}|$), which transforms each edge $e_i \in \mathcal{E}$ into a length- z vector $\mathbf{Z}[e_i]$ as its feature representation. Such a feature representation $\mathbf{Z}[e_i]$ should capture the rich semantics underlying both the bipartite graph structures and edge attributes. In this paper, we focus on the edge classification task, and thus, the edge representations are learned in a semi-supervised fashion by plugging the loss function for classifying edges into the model f .

3 THE EAGLE MODEL

As illustrated in Figure 2, we have developed two ERL models for EABG, i.e., EAGLE with FFP and dual-view FFP, both of which involve two key steps: k -truncated singular value decomposition (SVD) and feature propagation.

In this section, we focus on introducing our base EAGLE model, i.e., EAGLE with FFP. Section 3.1 first presents the objective of learning the edge-wise representations, while Section 3.2 then offers an in-depth analysis of the solution to the optimization objective. In Section 3.3, we elaborate on the feature propagation mechanism for computing the edge representations, followed by the loss function for the model training in Section 3.4.

3.1 Representation Learning Objective

Inspired by the numeric optimization analysis of generalized graph neural network models in recent studies [27, 53, 66], we formulate the ERL in EABGs as an optimization problem with consideration of the lopsided nature of bipartite graphs.

More concretely, EAGLE aims at achieving two goals: (i) the edge representations \mathbf{Z} close to the input edge feature matrix; and (ii) representations of edges that are incident to the same nodes should be similar. The former corresponds to a fitting term in the following equation:

$$O_f = \|\mathbf{Z} - f_\Theta(\mathbf{X})\|_F^2, \quad (2)$$

where $f_\Theta(\mathbf{X}) \in \mathbb{R}^{|\mathcal{E}| \times z}$ represents a non-linear transformation features of the input edge attribute matrix \mathbf{X} using an MLP $f_\Theta(\cdot)$ parameterized by a learnable weight matrix $\Theta \in \mathbb{R}^{d \times z}$ (including a nonlinear activation function ReLU operation and dropout operation), while the latter is a graph structure-based regularization term O_r defined by

$$O_r = \frac{\beta}{2} \sum_{u \in \mathcal{U}} \sum_{e_i, e_j \in \mathcal{E}_u} \frac{1}{|\mathcal{E}_u|} \cdot \|\mathbf{Z}[e_i] - \mathbf{Z}[e_j]\|^2 + \frac{1-\beta}{2} \sum_{v \in \mathcal{V}} \sum_{e_i, e_j \in \mathcal{E}_v} \frac{1}{|\mathcal{E}_v|} \cdot \|\mathbf{Z}[e_i] - \mathbf{Z}[e_j]\|^2. \quad (3)$$

Intuitively, Eq. (3) forces representations $\mathbf{Z}[e_i], \mathbf{Z}[e_j]$ to be close in the Euclidean space if their corresponding edges e_i, e_j are correlated to common nodes. $\frac{1}{|\mathcal{E}_u|}$ (resp. $\frac{1}{|\mathcal{E}_v|}$) is the weight used to reflect the importance of e_i, e_j from the perspective of common node u (resp. v). In particular, we use coefficients β and $1 - \beta$ to control the importance of edge pairs' shared nodes from \mathcal{U} and \mathcal{V} in constraining the distance between the representations, respectively.

Table 1: Properties of \mathbf{P} ($\beta = 0.5$)

Dataset	σ_2	σ_2^2	$\frac{1}{1-\sigma_2^2}$	$\frac{1}{1-\alpha\sigma_k^2}$
AMiner	0.9997	0.9994	1574.3930	1.8207
OAG	0.9999	0.9997	3780.6051	1.8775

In sum, the objective of learning \mathbf{Z} can be formulated as follows:

$$\min_{\mathbf{Z} \in \mathbb{R}^{|\mathcal{E}| \times z}} (1 - \alpha) \cdot O_f + \alpha \cdot O_r, \quad (4)$$

where hyper-parameter α is to balance the above-said two terms.

3.2 Analysis of the Optimal Solution

LEMMA 3.1. *The closed-form solution to Eq. (4) is*

$$\mathbf{Z} = (1 - \alpha) \sum_{t=0}^{\infty} \alpha^t \mathbf{P}^t \cdot f_\Theta(\mathbf{X}), \quad (5)$$

where \mathbf{P} is an edge-wise transition matrix defined by

$$\mathbf{P} = \mathbf{E}\mathbf{D}^{-1}\mathbf{E}^\top, \quad \mathbf{E} = \sqrt{\beta} \cdot \mathbf{E}_\mathcal{U} \parallel \sqrt{1-\beta} \cdot \mathbf{E}_\mathcal{V}. \quad (6)$$

Lemma 3.1 offers a simple yet elegant way (i.e., Eq. (5)) to calculate the optimal edge representations \mathbf{Z} to the optimization objective in Eq. (4). However, Eq. (5) requires summing up an infinite series of matrix multiplications, which is infeasible in practice, especially for large EABGs. A remedy is to compute an approximate version \mathbf{Z}' by summing up at most $T + 1$ terms with a small integer T :

$$\mathbf{Z}' = (1 - \alpha) \sum_{t=0}^T \alpha^t \mathbf{P}^t \cdot f_\Theta(\mathbf{X}). \quad (7)$$

In what follows, we theoretically show that such a truncation is not a favorable choice in EABGs.

LEMMA 3.2. *Given \mathbf{P} in Eq. (6), $\mathbf{P} = \beta \cdot \mathbf{P}_\mathcal{U} + (1 - \beta) \cdot \mathbf{P}_\mathcal{V}$.*

First, by Lemma 3.2, \mathbf{P} is a linear combination of $\mathbf{P}_\mathcal{U}$ and $\mathbf{P}_\mathcal{V}$. Recall that both $\mathbf{P}_\mathcal{U}$ and $\mathbf{P}_\mathcal{V}$ are non-negative doubly stochastic, which further connotes that \mathbf{P} is *non-negative doubly stochastic* and can be regarded as a reversible Markov chain. Let T_{mix} be its mixing time. Using its doubly stochastic property and the Convergence Theorem in [22, 28], when $t > T_{mix}$, $\mathbf{P}^t f_\Theta(\mathbf{X})$ converges to a stationary distribution Π , wherein $\Pi[e_i]$ is a constant vector, i.e., $1 \cdot \|\mathbf{P}^t f_\Theta(\mathbf{X})[e_i]\|_1$. Thus, \mathbf{Z} in Eq. (5) can be broken down into two parts¹:

$$\left((1 - \alpha) \sum_{t=0}^{T_{mix}-1} \alpha^t \mathbf{P}^t \cdot f_\Theta(\mathbf{X}) \right) + \alpha^{T_{mix}} \Pi. \quad (8)$$

Intuitively, since each row in Π is a constant vector, $\alpha^{T_{mix}} \Pi$ is not an informative representation matrix. As such, Eq. (8) implies that if we pick a large T ($T \gg T_{mix}$) for \mathbf{Z}' , constant vectors $\alpha^{T_{mix}} \Pi$ might jeopardize the representation quality of \mathbf{Z}' in Eq. (7), especially on graphs with small mixing times, resulting in degraded performance. On the other hand, a small T ($T \ll T_{mix} - 1$) for \mathbf{Z}' fails to enable an adequate preservation of the topological semantics underlying the input EABGs.

LEMMA 3.3. *Let σ_2 be the second largest singular value of $\mathbf{E}\mathbf{D}^{-1/2}$ (defined in Eq. (6)), $T_{mix} \geq \frac{1}{1-\sigma_2^2} - 1$.*

¹For the interest of space, we defer all proofs to Appendix A.

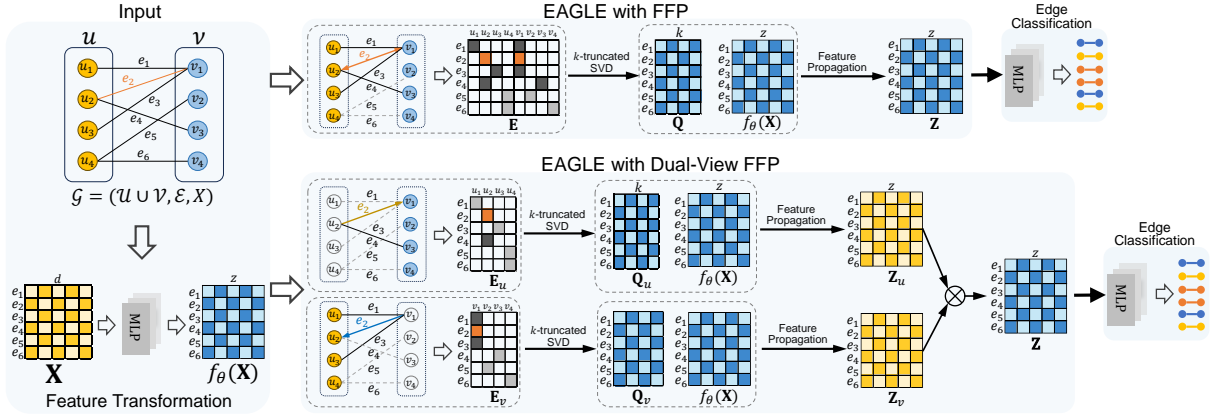


Figure 2: The overall framework of EAGLE

Lemma 3.3 provides a lower bound for T_{mix} , which is proportional to the inverse of $1 - \sigma_2^2$. As per the empirical data on real EABGs (see Section 5.2) from Table 1, σ_2 is notably approaching 1, rendering T_{mix} extremely large (over thousands), as a consequence of the unique characteristics of bipartite graph structures. We can conclude that the $\alpha^{T_{mix}} \Pi$ part in \mathbf{Z} (Eq. (8)) is insignificant. Additionally, based on Section 12.2 in [22], given any integer t and any edge $e_i \in \mathcal{E}$,

$$\text{Var}_{\Pi[e_i]}(\mathbf{P}^t f_{\Theta}(\mathbf{X})[e_i]) \leq \sigma_2^{4t} \cdot \text{Var}_{\Pi[e_i]}(f_{\Theta}(\mathbf{X})[e_i]),$$

where $\text{Var}_{\Pi[e_i]}$ stands for the variance computed w.r.t. the stationary distribution $\Pi[e_i]$. Since σ_2 is almost 1, the above equation manifests that even for a very large t , the difference between $\mathbf{P}^t f_{\Theta}(\mathbf{X})[e_i]$ and the stationary distribution $\Pi[e_i]$ can be as significant as that of the input feature vector $f_{\Theta}(\mathbf{X})[e_i]$. That is to say, $\mathbf{P}^t f_{\Theta}(\mathbf{X})[e_i]$ with large t still encompasses rich and informative features, and thus, computing \mathbf{Z} via Eq. (7) leads to compromised representation quality.

3.3 Factorized Feature Propagation

However, it remains tenaciously challenging to calculate the edge representations \mathbf{Z} by Eq. (5). To tackle this issue, we resort to a dimensionality reduction approach, dubbed as *factorized feature propagation* (FFP). The rudimentary idea behind FFP is to construct an $|\mathcal{E}| \times k$ ($k \ll |\mathcal{E}|$) matrix \mathbf{Q} such that $\mathbf{Q} \cdot \mathbf{Q}^T \approx (1 - \alpha) \sum_{t=0}^{\infty} \alpha^t \mathbf{P}^t$ without explicitly materializing $(1 - \alpha) \sum_{t=0}^{\infty} \alpha^t \mathbf{P}^t$. As such, edge representations \mathbf{Z} in Eq. (5) can be approximated via

$$\mathbf{Z} = \mathbf{Q} \cdot (\mathbf{Q}^T f_{\Theta}(\mathbf{X})), \quad (9)$$

which can be done in $O(|\mathcal{E}| \cdot kz)$ time. To realize the above idea, FFP first conducts a k -truncated SVD over $\mathbf{E} \mathbf{D}^{-\frac{1}{2}}$ to get its left singular vectors \mathbf{U} and the diagonal matrix Σ containing singular values. Then, we construct \mathbf{Q} as

$$\mathbf{Q} = \mathbf{U} \cdot \sqrt{\frac{1}{1 - \alpha \Sigma^2}}. \quad (10)$$

The underlying rationale is on the basis of $\mathbf{P} = \mathbf{E} \mathbf{D}^{-\frac{1}{2}} \cdot (\mathbf{E} \mathbf{D}^{-\frac{1}{2}})^T \approx \mathbf{U} \Sigma^2 \mathbf{U}^T$. The result in Eq. (10) is a direct inference after proving all

singular values of $\mathbf{E} \mathbf{D}^{-\frac{1}{2}}$ not greater than 1 in Lemma A.1:

$$(1 - \alpha) \sum_{t=0}^{\infty} \alpha^t \mathbf{P}^t \approx \mathbf{U} \cdot \sum_{t=0}^{\infty} \alpha^t \cdot \Sigma^{2t} \cdot \mathbf{U}^T = \mathbf{U} \cdot \frac{1}{1 - \alpha \Sigma^2} \cdot \mathbf{U}^T.$$

Correctness Analysis. Theorem 3.4 establishes the approximation accuracy guarantees of \mathbf{Q} . In practice, we usually set $k = 256$, and thus, the total error sum $\frac{1}{1 - \alpha \sigma_k^2}$ is roughly 2, as reported in Table 1.

THEOREM 3.4. *Let \mathbf{Q} be the $|\mathcal{E}| \times k$ matrix defined in Eq. (10) and σ_k be the k -th largest singular value of $\mathbf{E} \mathbf{D}^{-\frac{1}{2}}$. Then, the following inequality holds*

$$\left\| \mathbf{Q} \mathbf{Q}^T - (1 - \alpha) \sum_{t=0}^{\infty} \alpha^t \mathbf{P}^t \right\|_F \leq \frac{1}{1 - \alpha \sigma_k^2}.$$

In particular, when $k = |\mathcal{E}|$,

$$\mathbf{Q} \mathbf{Q}^T = (1 - \alpha) \sum_{t=0}^{\infty} \alpha^t \mathbf{P}^t.$$

Complexity Analysis. As remarked earlier, Eq. (9) consumes $O(|\mathcal{E}| \cdot kz)$ time. According to [12], the k -truncated SVD of sparse matrix $\mathbf{E} \mathbf{D}^{-\frac{1}{2}}$ (comprising $2|\mathcal{E}|$ elements) takes $O(|\mathcal{E}| \cdot k^2 + k^3)$ time when the randomized algorithm is employed. Overall, the total computational cost incurred by FFP is bounded by $O(|\mathcal{E}|k \cdot (k + z))$.

3.4 Model Training

In this work, we mainly focus on the semi-supervised edge classification task. The edge representations \mathbf{Z} output by FFP are subsequently fed into an MLP network $f_{\Omega}(\cdot)$ to yield the edge classification result:

$$\mathbf{Y} = \text{sigmoid}(f_{\Omega}(\mathbf{Z})) \in \mathbb{R}^{|\mathcal{E}| \times |C|} \quad (11)$$

where $|C|$ is the number of classes and f_{Ω} is parameterized by a learnable weight matrix $\Omega \in \mathbb{R}^{k \times |C|}$, followed by a nonlinear activation function ReLU operation and a dropout operation. In sum, the trainable parameters of EAGLE are only the weight matrix $\Theta \in \mathbb{R}^{d \times z}$ in the feature transformation layer $f_{\Theta}(\mathbf{X})$ and the weight matrix $\Omega \in \mathbb{R}^{k \times |C|}$ of the output layer in Eq. (11).

Following common practice, we employ the cross-entropy loss with ground-truth edge labels to guide the model training:

$$\mathcal{L} = -\frac{1}{|\mathcal{E}_L|} \sum_{e_i \in \mathcal{E}_L} \sum_{j \in \mathcal{C}} \widehat{Y}[e_i, j] \cdot \log(Y[e_i, j]) + (1 - \widehat{Y}[e_i, j]) \cdot \log(1 - Y[e_i, j]),$$

where \mathcal{E}_L denotes the set of labeled edges, \widehat{Y} consists of the ground-truth labels of edges ($\widehat{Y}[e_i, j] = 1$ if e_i belongs to class C_j and 0 otherwise), and $Y[e_i, j]$ stands for the predicted probability of edge e_i belonging to class C_j .

4 EAGLE WITH DUAL-VIEW FFP

Recall that in Section 3.2, the edge-wise transition matrix \mathbf{P} can be equivalently converted into $\mathbf{P} = \beta \cdot \mathbf{P}_{\mathcal{U}} + (1 - \beta) \cdot \mathbf{P}_{\mathcal{V}}$ (Lemma 3.2). In turn, the edge representations \mathbf{Z} in Eq. (5) are essentially obtained through a linear combination of the features propagated between edges via their connections using two heterogeneous node sets \mathcal{U} and \mathcal{V} as intermediaries, which tends to yield sub-optimal representation effectiveness. Further, such a linear combination relies on a manually selected parameter β to balance the importance of features w.r.t. these two views, which requires re-calculating the k -truncated SVD of $\mathbf{E}\mathbf{D}^{-\frac{1}{2}}$ (see Eq. (6)) from scratch to create \mathbf{Q} (Eq. (10)) once β was changed, leading to significant computation effort.

To mitigate the foregoing issues, in EAGLE, we develop *dual-view factorized feature propagation* (referred to as DV-FFP) for learning enhanced edge representations. The basic idea is to create two intermediate edge representations, $\mathbf{Z}_{\mathcal{U}}$ and $\mathbf{Z}_{\mathcal{V}}$, by utilizing the associations between edges from the views of \mathcal{U} and \mathcal{V} severally, and then coalesce them into the final edge representations \mathbf{Z} .

In the sequel, Section 4.1 elaborates on the details of DV-FFP, followed by a theoretical analysis in Section 4.2

4.1 Dual-View Factorized Feature Propagation

Akin to Eq. (5), the goal of DV-FFP is to generate edge representations $\mathbf{Z}_{\mathcal{U}}$ and $\mathbf{Z}_{\mathcal{V}}$ from the \mathcal{U} -wise and \mathcal{V} -wise views as follows:

$$\begin{aligned} \mathbf{Z}_{\mathcal{U}} &= (1 - \alpha) \sum_{t=0}^{\infty} \alpha^t \mathbf{P}_{\mathcal{U}}^t \cdot f_{\Theta_{\mathcal{U}}}(\mathbf{X}), \\ \mathbf{Z}_{\mathcal{V}} &= (1 - \alpha) \sum_{t=0}^{\infty} \alpha^t \mathbf{P}_{\mathcal{V}}^t \cdot f_{\Theta_{\mathcal{V}}}(\mathbf{X}). \end{aligned} \quad (12)$$

In Eq. (12), $f_{\Theta_{\mathcal{U}}}(\mathbf{X})$ (resp. $f_{\Theta_{\mathcal{V}}}(\mathbf{X})$) corresponds to the initial edge features used for the generation of $\mathbf{Z}_{\mathcal{U}}$ (resp. $\mathbf{Z}_{\mathcal{V}}$), which is transformed from the input edge attribute vectors \mathbf{X} through an MLP network parameterized by weight matrix $\Theta_{\mathcal{U}}$ (resp. $\Theta_{\mathcal{V}}$).

In analogy to FFP in Section 3.3, DV-FFP adopts a low-dimensional matrix approximation trick to approximate $(1 - \alpha) \sum_{t=0}^{\infty} \alpha^t \mathbf{P}_{\mathcal{U}}^t$ and $(1 - \alpha) \sum_{t=0}^{\infty} \alpha^t \mathbf{P}_{\mathcal{V}}^t$, while sidestepping the explicit construction of these two $|\mathcal{E}| \times |\mathcal{E}|$ dense matrices. Specifically, DV-FFP first applies a k -truncated SVD over $\mathbf{E}_{\mathcal{U}}\mathbf{D}_{\mathcal{U}}^{-\frac{1}{2}}$ and $\mathbf{E}_{\mathcal{V}}\mathbf{D}_{\mathcal{V}}^{-\frac{1}{2}}$, respectively, to get the left singular vectors $\mathbf{U}_{\mathcal{U}}$, singular values $\Sigma_{\mathcal{U}}$, and their counterparts $\mathbf{U}_{\mathcal{V}}$ and $\Sigma_{\mathcal{V}}$. Let $\mathbf{Q}_{\mathcal{U}} = \mathbf{U}_{\mathcal{U}} \sqrt{\frac{1}{1 - \alpha \Sigma_{\mathcal{U}}^2}}$ and

$\mathbf{Q}_{\mathcal{V}} = \mathbf{U}_{\mathcal{V}} \sqrt{\frac{1}{1 - \alpha \Sigma_{\mathcal{V}}^2}}$. Then, the \mathcal{U} -wise and \mathcal{V} -wise edge representations $\mathbf{Z}_{\mathcal{U}}$ and $\mathbf{Z}_{\mathcal{V}}$ can be computed by

$$\mathbf{Z}_{\mathcal{U}} = \mathbf{Q}_{\mathcal{U}} \cdot \left(\mathbf{Q}_{\mathcal{U}}^{\top} f_{\Theta_{\mathcal{U}}}(\mathbf{X}) \right) \text{ and } \mathbf{Z}_{\mathcal{V}} = \mathbf{Q}_{\mathcal{V}} \cdot \left(\mathbf{Q}_{\mathcal{V}}^{\top} f_{\Theta_{\mathcal{V}}}(\mathbf{X}) \right), \quad (13)$$

respectively. Afterwards, they are combined as the final edge representations \mathbf{Z} through

$$\mathbf{Z} = f_{\text{combine}}(\gamma \cdot \mathbf{Z}_{\mathcal{U}}, (1 - \gamma) \cdot \mathbf{Z}_{\mathcal{V}}), \quad (14)$$

where $f_{\text{combine}}(\cdot, \cdot)$ is a combinator function, which can be a summation operator $+$, matrix concatenation operator \parallel , or max operator, and $\gamma \in [0, 1]$ is a hyper-parameter.

4.2 Analysis

In the rest of this section, we theoretically analyze the optimization objective of learning $\mathbf{Z}_{\mathcal{U}}$, $\mathbf{Z}_{\mathcal{V}}$ as in Eq. (12), the approximation accuracy guarantees of $\mathbf{Q}_{\mathcal{U}}$ and $\mathbf{Q}_{\mathcal{V}}$, as well as the computational expense of DV-FFP, respectively.

Optimization Objective. Recall that $\mathbf{P} = \beta \cdot \mathbf{P}_{\mathcal{U}} + (1 - \beta) \cdot \mathbf{P}_{\mathcal{V}}$ by Lemma 3.2. If we set β to 1 and 0, \mathbf{P} in Eq. (6) turns into $\mathbf{P}_{\mathcal{U}}$ and $\mathbf{P}_{\mathcal{V}}$, respectively. Accordingly, \mathbf{Z} defined in Eq. (5) becomes $\mathbf{Z}_{\mathcal{U}}$ and $\mathbf{Z}_{\mathcal{V}}$, if we replace $f_{\Theta}(\mathbf{X})$ by $f_{\Theta_{\mathcal{U}}}(\mathbf{X})$ and $f_{\Theta_{\mathcal{V}}}(\mathbf{X})$, respectively. Since Lemma 3.1 indicates that \mathbf{Z} in Eq. (5) is the closed solution to the objective in Eq. (4), when $\beta = 1$ or $\beta = 0$, $\mathbf{Z}_{\mathcal{U}}$ and $\mathbf{Z}_{\mathcal{V}}$ defined in Eq. (12) are thus the closed form solutions to the problems that minimize the following objectives:

$$\begin{aligned} (1 - \alpha) \|\mathbf{Z}_{\mathcal{U}} - f_{\Theta_{\mathcal{U}}}(\mathbf{X})\|_F^2 + \frac{\alpha}{2} \sum_{u \in \mathcal{U}} \sum_{e_i, e_j \in \mathcal{E}_u} \frac{1}{|\mathcal{E}_u|} \cdot \|\mathbf{Z}_{\mathcal{U}}[e_i] - \mathbf{Z}_{\mathcal{U}}[e_j]\|^2, \\ (1 - \alpha) \|\mathbf{Z}_{\mathcal{V}} - f_{\Theta_{\mathcal{V}}}(\mathbf{X})\|_F^2 + \frac{\alpha}{2} \sum_{v \in \mathcal{V}} \sum_{e_i, e_j \in \mathcal{E}_v} \frac{1}{|\mathcal{E}_v|} \cdot \|\mathbf{Z}_{\mathcal{V}}[e_i] - \mathbf{Z}_{\mathcal{V}}[e_j]\|^2, \end{aligned}$$

respectively.

Correctness. Since when we set $\beta = 1$ (resp. $\beta = 0$), \mathbf{P} and $\mathbf{E}\mathbf{D}^{-1/2}$ turn into $\mathbf{P}_{\mathcal{U}}$ and $\mathbf{E}_{\mathcal{U}}\mathbf{D}_{\mathcal{U}}^{-1/2}$ (resp. $\mathbf{P}_{\mathcal{V}}$ and $\mathbf{E}_{\mathcal{V}}\mathbf{D}_{\mathcal{V}}^{-1/2}$). Let $\sigma_k(\mathcal{U})$ and $\sigma_k(\mathcal{V})$ be the k -th largest singular value of $\mathbf{E}_{\mathcal{U}}\mathbf{D}_{\mathcal{U}}^{-1/2}$ and $\mathbf{E}_{\mathcal{V}}\mathbf{D}_{\mathcal{V}}^{-1/2}$, respectively. Based on Theorem 3.4, we can derive the following inequalities

$$\begin{aligned} \left\| \mathbf{Q}_{\mathcal{U}} \mathbf{Q}_{\mathcal{U}}^{\top} - (1 - \alpha) \sum_{t=0}^{\infty} \alpha^t \mathbf{P}_{\mathcal{U}}^t \right\|_F &\leq \frac{1}{1 - \alpha \sigma_k^2(\mathcal{U})}, \\ \left\| \mathbf{Q}_{\mathcal{V}} \mathbf{Q}_{\mathcal{V}}^{\top} - (1 - \alpha) \sum_{t=0}^{\infty} \alpha^t \mathbf{P}_{\mathcal{V}}^t \right\|_F &\leq \frac{1}{1 - \alpha \sigma_k^2(\mathcal{V})}. \end{aligned}$$

In particular, when $k = |\mathcal{E}|$,

$$\mathbf{Q}_{\mathcal{U}} \mathbf{Q}_{\mathcal{U}}^{\top} = (1 - \alpha) \sum_{t=0}^{\infty} \alpha^t \mathbf{P}_{\mathcal{U}}^t \text{ and } \mathbf{Q}_{\mathcal{V}} \mathbf{Q}_{\mathcal{V}}^{\top} = (1 - \alpha) \sum_{t=0}^{\infty} \alpha^t \mathbf{P}_{\mathcal{V}}^t.$$

Complexity. The computations of $\mathbf{Z}_{\mathcal{U}}$ and $\mathbf{Z}_{\mathcal{V}}$ in Eq. (13) need $O(|\mathcal{E}|kz)$ time, respectively. The randomized k -truncated SVD [12] of sparse matrices $\mathbf{E}_{\mathcal{U}}\mathbf{D}_{\mathcal{U}}^{-\frac{1}{2}}$ and $\mathbf{E}_{\mathcal{V}}\mathbf{D}_{\mathcal{V}}^{-\frac{1}{2}}$ requires $O(|\mathcal{E}| \cdot k^2 + k^3)$ time. Therefore, DV-FFP and FFP have the same time complexity $O(|\mathcal{E}|k \cdot (k + z))$.

Table 2: Edge-Attributed Bipartite Networks

Name	$ \mathcal{E} $	$ \mathcal{U} $	$ \mathcal{V} $	d	$ \mathcal{C} $
Amazon	359,425	25,939	14,061	768	3
AMiner	54,465	39,358	641	768	10
DBLP	243,960	33,503	6497	768	10
Google	564,831	32,788	7212	768	3
MAG	50,443	38,990	1,010	768	10

5 EXPERIMENTS

In this section, we empirically study the effectiveness of our proposed EAGLE models on real-world datasets in terms of edge classification. All experiments are conducted on a Linux machine powered by 4 AMD EPYC 7313 CPUs with 500GB RAM, and 1 NVIDIA RTX A5000 GPU with 24GB memory. The code and all datasets are available at <https://github.com/wanghewen/EAGLE> for reproducibility.

5.1 Baselines and Hyperparameters

We compare our proposed solutions against 9 competitors in terms of edge classification accuracy. The first category of baseline models consists of node-wise representation learning methods, including GCN [21], GraphSAGE [13], SGC [46], DGI [40], GAT [39], and GATv2 [3]. We initialize the embeddings of edge endpoints as the mean average of their connected edge attributes. Then, we apply these node-wise representation learning methods to update the node embeddings for the edge endpoints. Finally, we concatenate the embeddings of edge endpoints along with edge attributes to generate the corresponding edge embeddings. The second category of baseline models consists of edge-wise representation learning methods, including GEBE [56] and AttrE2Vec [2]. Additionally, we include a fully connected neural network (FC) to transform edge attributes without considering any network structure information.

For DGI, GEBE, and AttrE2Vec, we collect the source codes from the respective authors and adopt the parameter settings suggested in their papers to generate edge representations before feeding them to MLPs (multi-layer perceptrons) for classification. For GCN, GraphSAGE, SGC, GAT, and GATv2, we utilize the standard implementations provided in the well-known DGL² library and follow a three-layer neural network architecture, including two GNN layers and one linear layer, with ReLU as activation functions between layers. Besides, we set the dropout rate to 0.5 and the maximum number of training epochs to 300, and employ the Adam optimizer [20] for optimization with a learning rate of 0.001. All the methods are implemented in Python. In our solutions (i.e., EAGLE (FFP) and EAGLE (DV-FFP)), unless otherwise specified, we set the hyperparameter α and β to be 0.5, γ in Eq. (14) to be 0.5, and dimension k to be 256. The edge representations are then input to MLP classifiers to obtain the final edge labels. We report the AP/AUC on the test datasets using the model selected with the best AUC achieved on the cross-validation datasets.

5.2 Datasets

We use 5 real-world bipartite network datasets in the experiments. The Amazon dataset [29] contains user reviews for movies and TV

shows, where the edges represent the reviews written by users on the products, which are associated with labels representing users' ratings on these products. The Google dataset [23, 51] contains review information of business entities on Google Maps in Hawaii, United States, where the edges are reviews written by users on the business entity IDs. Similarly, the edge labels represent users' ratings on the business entities. AMiner [38], MAG [33, 59] and DBLP [37] datasets are 3 citation networks, in which nodes represent scholars and their publication venues of a paper. The edges represent the paper abstracts written for that paper. For AMiner, edge labels correspond to the keywords for the papers. For DBLP and MAG, edge labels correspond to the field of study for the papers. We select the most frequent 10 labels as targets to be predicted. To obtain initial edge features from text for these datasets, we apply the Sentence-BERT [32] model to encode text into 768-dimensional vectors. For each dataset, we use breadth-first search (BFS) to sample a smaller subset. Then we randomly split all edges into training, cross-validation and test sets with an 8 : 1 : 1 ratio. The properties and scales of the datasets used in our experiments are summarized in Table 2.

5.3 Edge Classification

Table 3 presents the edge classification performance of all methods on five datasets. Overall, our proposed methods consistently outperform all competitors on all five datasets. On review datasets like Amazon and Google, our method (EAGLE (DV-FFP)) using the max aggregator achieves approximately 0.9%-3.1% improvement in AP and approximately 0.4%-0.7% improvement in AUC compared to the best competitors. On citation network datasets like AMiner using keywords as edge labels, our method (EAGLE (FFP)) achieves around 177.5% improvement in AP and around 1.5% improvement in AUC compared to the best competitors. Note that most of the baselines cannot achieve high AP (below 0.2), due to the difficulties of classifying keywords in AMiner, as the number of keyword labels in the original dataset is much higher than the number of labels in the other datasets. On citation network datasets like DBLP and MAG using the field of study as edge labels, our method (EAGLE (DV-FFP)) using the max aggregator achieves approximately 7.1%-15.0% improvement in AP and approximately 1.2%-1.9% improvement in AUC compared to the best competitors. It is worth noting that for datasets like Amazon and AMiner, FC performs the best among the competitors. This indicates the difficulties of capturing the structural similarities in these graph datasets. However, our methods can still successfully generate better edge representations on these datasets. Another observation is that EAGLE (DV-FFP) outperforms EAGLE (FFP) and other competitors on four datasets out of five. This suggests the importance of introducing intermediate edge representation independently from the views of heterogeneous node sets $Z_{\mathcal{U}}$ and $Z_{\mathcal{V}}$.

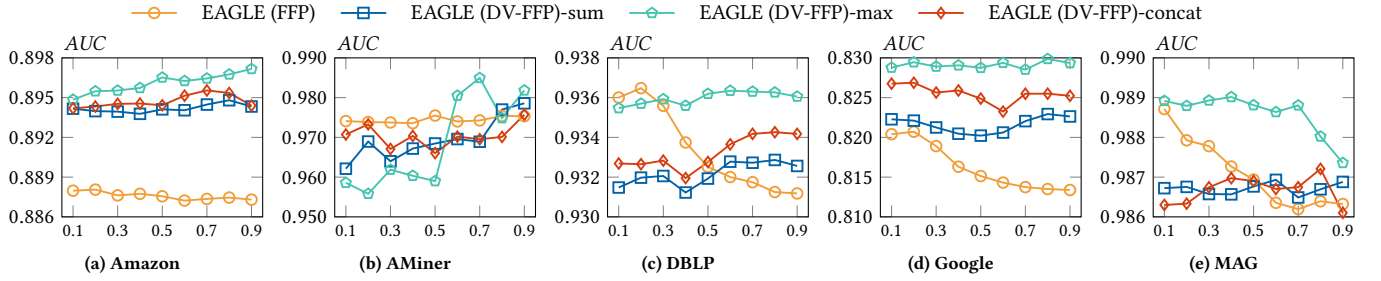
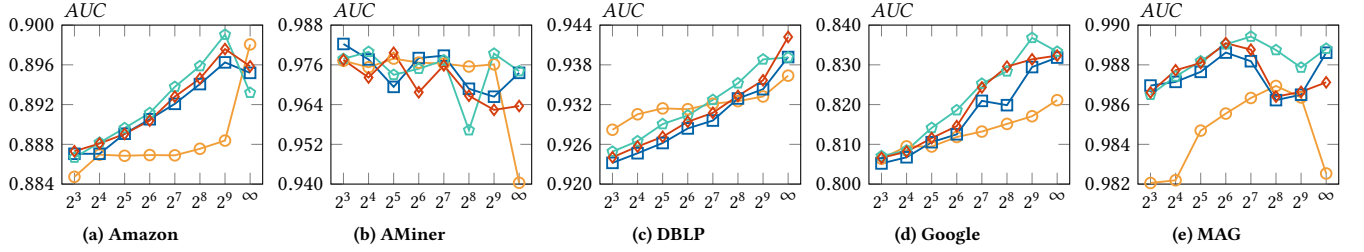
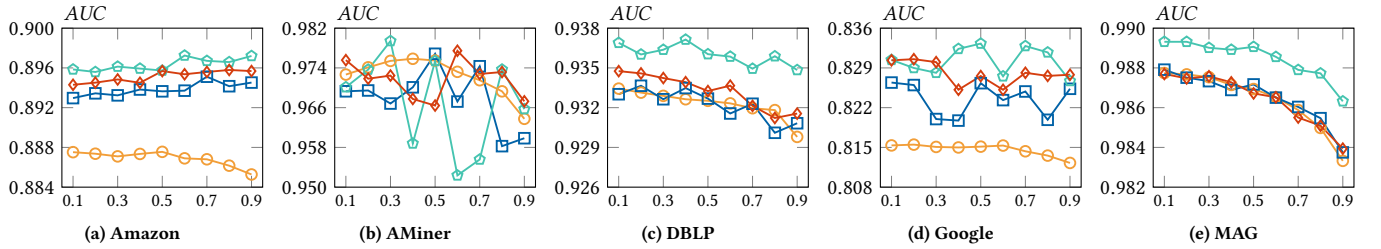
5.4 Parameter Analysis

In this section, we experimentally study the effects of varying three key parameters in our proposed method, including β used in Eq. (6), k for matrix \mathbf{Q} dimension, and α used in Eq. (4). We report the AUC scores by EAGLE (FFP) and EAGLE (DV-FFP) with three different aggregators when varying these parameters.

²<https://www.dgl.ai>

Table 3: Classification Performance (the higher the better).

Method	Amazon		AMiner		DBLP		Google		MAG	
	AP	AUC	AP	AUC	AP	AUC	AP	AUC	AP	AUC
GCN	0.6515	0.8691	0.0966	0.9254	0.5835	0.8979	0.5396	0.8122	0.7504	0.9617
GraphSAGE	0.6927	0.8874	0.1398	0.9485	<u>0.6785</u>	<u>0.9254</u>	<u>0.5789</u>	<u>0.8250</u>	<u>0.7998</u>	<u>0.9702</u>
SGC	0.5721	0.8203	0.0360	0.8468	0.4753	0.8576	0.4728	0.7563	0.6838	0.9470
DGI	0.3879	0.6094	0.0046	0.5024	0.2785	0.6813	0.3465	0.5336	0.4278	0.8315
GAT	0.6809	0.8810	0.1197	0.9077	0.5936	0.8988	0.5040	0.6928	0.7517	0.9614
GATv2	0.6871	0.8860	0.1356	0.9206	0.6462	0.9156	0.5313	0.7804	0.7673	0.9635
FC	<u>0.7030</u>	<u>0.8905</u>	<u>0.1877</u>	<u>0.9607</u>	0.6234	0.8922	0.5585	0.7890	0.7401	0.9564
GEBE	0.4751	0.7158	0.1013	0.8739	0.4164	0.8116	0.3956	0.6508	0.6555	0.9317
AttrE2Vec	0.3334	0.4991	0.0080	0.5966	0.1716	0.5390	0.3331	0.4976	0.1480	0.5463
EAGLE (FFP)	0.6946	0.8875	0.5209	0.9754	0.7069	0.9325	0.5787	0.8151	0.9047	0.9869
EAGLE (DV-FFP)-sum	0.7059	0.8941	0.5062	0.9684	0.7160	0.9319	0.5886	0.8202	0.9083	0.9867
EAGLE (DV-FFP)-max	<u>0.7093</u>	<u>0.8965</u>	0.3740	0.9589	<u>0.7267</u>	<u>0.9361</u>	<u>0.5968</u>	<u>0.8287</u>	<u>0.9195</u>	<u>0.9888</u>
EAGLE (DV-FFP)-concat	0.7064	0.8944	0.5081	0.9660	0.7187	0.9327	0.5931	0.8248	0.9128	0.9869

**Figure 3: Varying β in EAGLE (FFP) and γ in EAGLE (DV-FFP).****Figure 4: Varying k .****Figure 5: Varying α .**

In Figure 3, we report how AUC scores vary for different β for EAGLE (FFP) and different γ for EAGLE (DV-FFP). For Amazon, Google, and MAG, EAGLE (DV-FFP) with the max aggregator consistently performs the best across different β . For AMiner, the AUC scores reach the maximum when $\beta = 0.7$ and then decrease for EAGLE (DV-FFP) with max aggregator. For DBLP, the EAGLE (FFP)

performs the best when $\beta = 0.2$, but when $\beta \geq 0.3$, EAGLE (DV-FFP) with max aggregator becomes the best among all our methods. We can also observe that on DBLP, Google, and MAG, EAGLE (FFP) is more sensitive to the change of β compared with EAGLE (DV-FFP).

In Figure 4, we report how AUC scores vary for different SVD dimensions k . ∞ in Figure 4 refers to using power iteration to solve

for the edge embeddings. For Amazon, DBLP, and Google, the AUC scores of all our methods increase as k increases (excluding the solution from power iteration), as larger embedding dimensions can contain more graph structural information. For AMiner, AUC reaches the maximum when $k = 8$ for EAGLE (DV-FFP) using the sum aggregator. For MAG, AUC reaches the maximum for EAGLE (DV-FFP) using the max aggregator when $k = 128$ and then decreases.

In Figure 5, we report how AUC scores vary for different α . By tuning α , we observe that EAGLE (DV-FFP) with the max aggregator can achieve the best performance on these datasets compared with other methods. In particular, on Amazon, AMiner, DBLP, and Google, EAGLE (DV-FFP) with the max aggregator performs best with α value between 0.3 and 0.6. On MAG, EAGLE (DV-FFP) with the max aggregator shows a decreasing trend as α increases. As mentioned in Section 3.1, α balances the importance between the edge representations derived from edge features and graph structures. This suggests on MAG, our methods can achieve improvements by a careful trade-off between edge attributes and graph structures.

6 RELATED WORK

This section reviews existing graph node/edge representation learning on unipartite/bipartite graphs, as well as their applications.

6.1 Node-wise Representation Learning

Node-wise GRL refers to the process of generating embeddings for the nodes of a graph. Conventional approaches for addressing this task involve methods based on matrix factorization and random walk. In matrix factorization-based methods, such as HOPE [30], AROPE [63], PRONE [61], NRP [57], PANE [58], and SketchNE [1], a proximity-based matrix \mathbf{P} is initially created for the graph, where each element $\mathbf{P}[i, j]$ denotes the proximity measure between nodes i and j . Subsequently, a dimension reduction technique is employed to derive lower-dimensional representations for the nodes. In random walk-based methods, such as Deepwalk [31], LINE [36], and node2vec [11], the process begins with the generation of random walks for each node to capture the underlying graph structures. Subsequently, the co-occurrence in these random walks is employed to assess node similarities and generate node embedding vectors.

Another line of research lies in graph neural networks (GNNs). The major categories of GNNs, for example, GCN [21], GraphSAGE [13], SGC [46], DGI [40], GAT [39], and GATv2 [3], adopt ideas from convolutional neural networks for modeling graph-structured data. GNNs aggregate local neighborhood information to get contextual representation for graph nodes and have shown promising results in this area. To consider the effect of edge attributes, some new GNN models are proposed to incorporate them during the training process. EGAT [45] proposes edge-featured graph attention layers that can accept node and edge features as inputs and handle them spontaneously within the models. GERI [35] constructs a heterogeneous graph using the attribute information and applies random walk with a modified heterogeneous skip-gram to learn node embeddings. EEGNN [26] proposes a framework called edge-enhanced graph neural network that uses the structural information extracted from a Bayesian nonparametric model for graphs to consider the effect of self-loops and multiple

edges between two nodes and improve the performance of various deep message-passing GNNs. EGNN [10] uses multi-dimensional nonnegative-valued edge features represented as a tensor and applies GCN/GAT to exploit multiple attributes associated with each edge. GraphBEAN [5] applies autoencoders on bipartite graphs with both node and edge attributes to obtain node embeddings for node and edge level anomaly detection.

6.2 Edge-wise Representation Learning

Edge-wise GRL refers to the process of generating embeddings for edges of a graph. [24] uses random walks to sample a series of edge sequences to generate edge embeddings and apply clustering algorithms for community detection. Edge2Vec [6] uses deep auto-encoders and skip-gram models to generate edge embeddings that preserve both the local and global structure information of edges for biomedical knowledge discovery. AttrE2Vec [2] generates random walks starting from a node and uses aggregation functions to aggregate node/edge features in the random walks and obtain node/edge representations. Then, it uses auto-encoders and self-attention networks with feature reconstruction loss and graph structural loss to build edge embeddings in an unsupervised manner. [42] uses matrix factorization and feature aggregation to generate edge representation vectors based on the graph structure surrounding edges and edge attributes, which can encode high-order proximities of edges and edge attribute information into low-dimensional vectors. CEN-DGCNN [65] introduces a deep graph convolutional neural network that integrates node and edge features, preventing over-smoothing. It captures non-local structural features and refines high-order node features by considering long-distance dependencies and multi-dimensional edge features. DoubleFA [43] proposes to use top-k Personalized PageRank to conduct proximal feature aggregation and anomaly feature aggregation using edge features for edge anomaly detection.

6.3 Bipartite Graph Representation Learning

For a comprehensive review of existing bipartite graph representation learning methods, we suggest readers check [8]. BiANE [18] employs auto-encoders to model inter-partition and intra-partition proximity using attribute proximity and structure proximity through a latent correlation training approach. Cascade-BGNN [15] utilizes customized inter-domain message passing and intra-domain alignment with adversarial learning for message aggregation across and within graph partitions. BiGI [4] utilizes GCN to generate initial node embeddings and applies a subgraph-level attention mechanism to maximize the mutual information between local and global node representations. DualHGNN [50] transforms the multiplex bipartite network into two sets of homogeneous hypergraphs and uses spectral hypergraph convolutional operators to capture information within and across domains. GEBE [56] proposes proximity matrices derived from the edge weight matrix and applies matrix factorization to capture multi-hop similarity/proximity between homogeneous/heterogeneous nodes. AnchorGNN [47] proposes a global-local learning framework that leverages an anchor-based message-passing schema to generate node embeddings for large bipartite graphs.

7 CONCLUSIONS

In this work, we introduce the problem of ERL on EABGs and propose EAGLE models to address this problem. Building on an in-depth theoretical analysis of extending the feature propagation paradigm in GNNs to ERL on EABGs, we design the FFP scheme that is able to effectively capture long-range dependencies between edges for generating high-quality edge representations without entailing vast computational costs. On the basis of FFP, we propose the dual-view FFP by leveraging the semantics of two sets of heterogeneous nodes in the input bipartite graphs to enhance edge representations. The effectiveness of our proposed EAGLE models is validated by our extensive experiments comparing EAGLE against nine baselines over five real datasets.

ACKNOWLEDGMENTS

This research is supported by the Ministry of Education, Singapore, under its MOE AcRF TIER 3 Grant (MOE-MOET32022-0001). Any opinions, findings and conclusions or recommendations expressed in this material are those of the author(s) and do not reflect the views of the Ministry of Education, Singapore. Renchi Yang is supported by the NSFC Young Scientists Fund (No. 62302414) and the Hong Kong RGC ECS grant (No. 22202623).

A PROOFS

Proof of Lemma 2.2. We first prove that $\mathbf{P}_{\mathcal{U}}$ is a row-stochastic matrix. Since it is symmetric, then its doubly stochastic property naturally follows. By Eq. (1), the (i, j) -th entry of $\mathbf{P}_{\mathcal{U}}$ is

$$\sum_{e_j \in \mathcal{E}} \mathbf{P}_{\mathcal{U}}[e_i, e_j] = \sum_{e_j \in \mathcal{E}} \frac{1}{\mathbf{D}[u^{(i)}, u^{(i)}] \cdot \mathbb{1}_{u^{(i)} \in e_j}} = 1,$$

where $\mathbb{1}_{u^{(i)} \in e_j}$ is an indicator function which equals 1 when node $u^{(i)}$ is an endpoint of edge e_j . A similar proof can be done for $\mathbf{P}_{\mathcal{V}}$. \square

LEMMA A.1. *If σ_1 be the largest singular value of $\mathbf{E}\mathbf{D}^{-\frac{1}{2}}$, $\sigma_1 \leq 1$.*

PROOF. According to [34], The singular values are the square roots of the non-zero eigenvalues of $\mathbf{E}\mathbf{D}^{-\frac{1}{2}} \cdot (\mathbf{E}\mathbf{D}^{-\frac{1}{2}})^\top = \mathbf{P}$. This implies that all the eigenvalues of \mathbf{P} are non-negative. Thus, $\sigma_1 = \sqrt{\lambda_1}$, where λ_1 is the largest eigenvalue of \mathbf{P} . Recall that \mathbf{P} is doubly stochastic. Then, we have

$$\|\mathbf{P}\|_\infty = \max_{1 \leq i \leq |\mathcal{E}|} \sum_{j=1}^{|\mathcal{E}|} \mathbf{P}_{i,j} = 1.$$

By Theorem 5.6.9 in [16],

$$|\lambda_1| \leq \rho(\mathbf{P}) \leq \|\mathbf{P}\|_\infty = 1,$$

where $\rho(\mathbf{P})$ is the spectral radius of \mathbf{P} , which leads to $\sigma_1 \leq 1$. \square

Lemma 3.1. First, it is easy to derive that Eq. 3 can be transformed to its equivalent form $\mathcal{O}_r = \text{trace}(\mathbf{Z}^\top (\mathbf{I} - \mathbf{P})\mathbf{Z})$. Accordingly, Eq. 4 is converted into

$$(1 - \alpha) \cdot \|\mathbf{Z} - f_\Theta(\mathbf{X})\|_F^2 + \alpha \cdot \text{trace}(\mathbf{Z}^\top (\mathbf{I} - \mathbf{P})\mathbf{Z}).$$

By setting its derivative w.r.t. \mathbf{Z} to zero, we obtain the optimal \mathbf{Z} as:

$$\begin{aligned} \frac{\partial \{(1 - \alpha) \cdot \|\mathbf{Z} - \mathbf{X}\|_F^2 + \alpha \cdot \text{trace}(\mathbf{Z}^\top (\mathbf{I} - \mathbf{P})\mathbf{Z})\}}{\partial \mathbf{Z}} &= 0 \\ \implies (1 - \alpha) \cdot (\mathbf{Z} - f_\Theta(\mathbf{X})) + \alpha (\mathbf{I} - \mathbf{P})\mathbf{Z} &= 0 \\ \implies \mathbf{Z} &= (1 - \alpha) \cdot (\mathbf{I} - \alpha\mathbf{P})^{-1} \cdot f_\Theta(\mathbf{X}). \end{aligned} \quad (15)$$

By the definition of Neumann series, i.e., $(\mathbf{I} - \mathbf{M})^{-1} = \sum_{t=0}^{\infty} \mathbf{M}^t$, we have

$$(\mathbf{I} - \alpha\mathbf{P})^{-1} = \sum_{t=0}^{\infty} \alpha^t \cdot \mathbf{P}^t.$$

Plugging the above equation into Eq. (15) completes the proof. \square

Proof of Lemma 3.2. Recall that \mathbf{D} can be represented by

$$\left(\begin{array}{c|c} \mathbf{D}_{\mathcal{U}} & \mathbf{0} \\ \hline \mathbf{0} & \mathbf{D}_{\mathcal{V}} \end{array} \right)$$

Then, as per Eq. (6), we have

$$\begin{aligned} \mathbf{P} &= (\sqrt{\beta}\mathbf{E}_{\mathcal{U}} \parallel \sqrt{1 - \beta}\mathbf{E}_{\mathcal{V}}) \cdot \mathbf{D}^{-1} \cdot (\sqrt{\beta}\mathbf{E}_{\mathcal{U}} \parallel \sqrt{1 - \beta}\mathbf{E}_{\mathcal{V}})^\top \\ &= \left(\sqrt{\beta}\mathbf{E}_{\mathcal{U}}\mathbf{D}_{\mathcal{U}}^{-\frac{1}{2}} \parallel \sqrt{1 - \beta}\mathbf{E}_{\mathcal{V}}\mathbf{D}_{\mathcal{V}}^{-\frac{1}{2}} \right) \cdot \left(\sqrt{\beta}\mathbf{E}_{\mathcal{U}}\mathbf{D}_{\mathcal{U}}^{-\frac{1}{2}} \parallel \sqrt{1 - \beta}\mathbf{E}_{\mathcal{V}}\mathbf{D}_{\mathcal{V}}^{-\frac{1}{2}} \right)^\top \\ &= \beta \cdot \mathbf{E}_{\mathcal{U}}\mathbf{D}_{\mathcal{U}}^{-1}\mathbf{E}_{\mathcal{U}}^\top + (1 - \beta) \cdot \mathbf{E}_{\mathcal{V}}\mathbf{D}_{\mathcal{V}}^{-1}\mathbf{E}_{\mathcal{V}}^\top \\ &= \beta \cdot \mathbf{P}_{\mathcal{U}} + (1 - \beta) \cdot \mathbf{P}_{\mathcal{V}}, \end{aligned}$$

which finishes the proof. \square

Proof of Eq. (8). According to Eq. (5), we have

$$\left((1 - \alpha) \sum_{t=0}^{T_{\text{mix}}-1} \alpha^t \mathbf{P}^t \cdot f_\Theta(\mathbf{X}) \right) + \left((1 - \alpha) \sum_{t=T_{\text{mix}}}^{\infty} \alpha^t \mathbf{\Pi} \right).$$

Note that we can rewrite the second part as:

$$\begin{aligned} (1 - \alpha) \sum_{t=T_{\text{mix}}}^{\infty} \alpha^t \mathbf{\Pi} &= \left((1 - \alpha) \sum_{t=0}^{\infty} \alpha^t - (1 - \alpha) \sum_{t=0}^{T_{\text{mix}}-1} \alpha^t \right) \cdot \mathbf{\Pi} \\ &= (1 - (1 - \alpha^{T_{\text{mix}}})) \cdot \mathbf{\Pi} = \alpha^{T_{\text{mix}}} \mathbf{\Pi}. \end{aligned}$$

Eq. (8) naturally follows. \square

Proof of Lemma 3.3. We first prove that σ_2^2 is the second largest eigenvalue of \mathbf{P} . By Eq. (6), $\mathbf{P} = (\mathbf{E}\mathbf{D}^{-1/2}) \cdot (\mathbf{E}\mathbf{D}^{-1/2})^\top$, which indicates that the eigenvalues of \mathbf{P} are the squared singular values of $\mathbf{E}\mathbf{D}^{-1/2}$ [16, 34]. Since singular values are non-negative, the second largest eigenvalue of \mathbf{P} is σ_2^2 . According to the fact of \mathbf{P} is a reversible Markov chain and Theorem 12.5 in [22], T_{mix} satisfies $T_{\text{mix}} \geq \frac{1}{1 - \sigma_2^2} - 1$. \square

Proof of Theorem 3.4. We first consider that $\mathbf{U}\mathbf{\Sigma}\mathbf{V}^\top$ is the exact full SVD of $\mathbf{E}\mathbf{D}^{-1/2}$. According to Lemma A.1, we can get

$$\mathbf{Q}\mathbf{Q}^\top = \mathbf{U} \cdot \frac{1}{1 - \alpha\mathbf{\Sigma}^2} \cdot \mathbf{U}^\top = \sum_{t=0}^{\infty} \alpha^t \cdot \mathbf{U} \cdot (\mathbf{\Sigma}^2)^t \cdot \mathbf{U}^\top.$$

Since \mathbf{U} and \mathbf{V} are semi-unitary matrices, i.e., $\mathbf{U}^\top \mathbf{U}$ and $\mathbf{V}^\top \mathbf{V}$,

$$\begin{aligned} \mathbf{Q}\mathbf{Q}^\top &= (1-\alpha) \sum_{t=0}^{\infty} \alpha^t (\mathbf{U}\Sigma^2\mathbf{U}^\top)^t = \sum_{t=0}^{\infty} \alpha^t (\mathbf{U}\Sigma \cdot (\mathbf{V}^\top \mathbf{V}) \cdot \Sigma\mathbf{U}^\top)^t \\ &= (1-\alpha) \sum_{t=0}^{\infty} \alpha^t (\mathbf{E}\mathbf{D}^{-\frac{1}{2}} \cdot (\mathbf{E}\mathbf{D}^{-\frac{1}{2}})^\top)^t \\ &= (1-\alpha) \sum_{t=0}^{\infty} \alpha^t (\mathbf{E}\mathbf{D}^{-1}\mathbf{E}^\top)^t = (1-\alpha) \sum_{t=0}^{\infty} \alpha^t \mathbf{P}^t. \end{aligned}$$

According to [16, 34], the definition of \mathbf{P} in Eq. (6) (i.e., $\mathbf{P} = \mathbf{E}\mathbf{D}^{-1/2} \cdot (\mathbf{E}\mathbf{D}^{-1/2})^\top$) implies that the singular values of $\mathbf{E}\mathbf{D}^{-1/2}$ are the square roots of the eigenvalues of \mathbf{P} , and the left singular vectors of $\mathbf{E}\mathbf{D}^{-1/2}$ are the eigenvectors of \mathbf{P} . In particular, due to the non-negativity of singular values, the k -th largest eigenvalue of \mathbf{P} is equal to σ_k^2 where σ_k denotes the k -th largest singular value of $\mathbf{E}\mathbf{D}^{-1/2}$.

Recall that \mathbf{P} is doubly stochastic, meaning that \mathbf{P} is a symmetric matrix. Using Theorem 4.1 in [63], we can derive that the singular values of \mathbf{P} are the absolute values of the corresponding eigenvalues, and the left singular vectors of \mathbf{P} are equal to the eigenvectors of \mathbf{P} . Since all the eigenvalues of \mathbf{P} are non-negative, its k -th largest eigenvalue is equal to the k -th largest singular value of \mathbf{P} .

Combining the above two conclusions, we can extrapolate that the k -th largest singular value of \mathbf{P} is equal to σ_k^2 , and the left singular vectors of $\mathbf{E}\mathbf{D}^{-1/2}$ are the left singular vectors of \mathbf{P} .

THEOREM A.2 (ECKART–YOUNG THEOREM [9]). *Suppose that $\mathbf{M}_k \in \mathbb{R}^{n \times k}$ is the rank- k approximation to $\mathbf{M} \in \mathbb{R}^{n \times n}$ obtained by exact SVD, then*

$$\min_{\text{rank}(\tilde{\mathbf{M}}) \leq k} \|\mathbf{M} - \tilde{\mathbf{M}}\|_F = \|\mathbf{M} - \mathbf{M}_k\|_F = \sigma_{k+1},$$

where σ_i represents the i -th largest singular value of \mathbf{M} .

Let $\mathbf{U}\Sigma\mathbf{V}^\top$ be the exact top- k SVD of $\mathbf{E}\mathbf{D}^{-1/2}$. Then, $\mathbf{U}\Sigma^2\mathbf{U}^\top$ is the exact top- k SVD of \mathbf{P} . By leveraging Eckart–Young Theorem in Theorem A.2, we obtain

$$\|\mathbf{U}\Sigma^2\mathbf{U}^\top - \mathbf{P}\|_F \leq \sigma_k^2.$$

Next, we prove that \mathbf{U} and $\frac{1}{1-\alpha\Sigma^2}$ are the top- k left singular vectors and singular values of $(1-\alpha) \sum_{t=0}^{\infty} \alpha^t \mathbf{P}^t$, respectively. We assume $k = |\mathcal{E}|$, which means

$$\mathbf{U} \frac{1}{1-\alpha\Sigma^2} \mathbf{U}^\top = (1-\alpha) \sum_{t=0}^{\infty} \alpha^t \mathbf{P}^t.$$

Consider vector $\mathbf{U}[:, i]$ and scalar $\frac{1}{1-\alpha\Sigma[i, i]^2}$ and denote by \mathbf{e}_i a one-hot vector. We can derive

$$\begin{aligned} (1-\alpha) \sum_{t=0}^{\infty} \alpha^t \mathbf{P}^t \cdot \mathbf{U}[:, i] &= \mathbf{U} \frac{1}{1-\alpha\Sigma^2} \mathbf{U}^\top \cdot \mathbf{U}[:, i] \\ &= \mathbf{U} \frac{1}{1-\alpha\Sigma^2} \cdot \mathbf{e}_i \\ &= \frac{1}{1-\alpha\Sigma[i, i]^2} \cdot \mathbf{U}[:, i]. \end{aligned}$$

In addition, by Lemma A.1, $\frac{1}{1-\alpha\Sigma[i, i]^2}$ is non-negative and is monotonically decreasing with i . As a consequence, we can conclude that

$\mathbf{U}[:, i]$ and scalar $\frac{1}{1-\alpha\Sigma[i, i]^2}$ are an eigenpair of $(1-\alpha) \sum_{t=0}^{\infty} \alpha^t \mathbf{P}^t$, and thus, its i -th largest left singular vector and singular value. Then, using Theorem A.2 yields

$$\begin{aligned} \|\mathbf{Q}\mathbf{Q}^\top - (1-\alpha) \sum_{t=0}^{\infty} \alpha^t \mathbf{P}^t\|_F &= \|\mathbf{U} \frac{1}{1-\alpha\Sigma^2} \mathbf{U}^\top - (1-\alpha) \sum_{t=0}^{\infty} \alpha^t \mathbf{P}^t\|_F \\ &\leq \frac{1}{1-\alpha\sigma_k^2}, \end{aligned}$$

which finishes the proof. \square

REFERENCES

- [1] 2023. SketchNE: Embedding Billion-Scale Networks Accurately in One Hour. *IEEE Transactions on Knowledge and Data Engineering* 35, 10 (oct 2023), 10666–10680. <https://doi.org/10.1109/TKDE.2023.3255703>
- [2] Piotr Bielak, Tomasz Kajdanowicz, and Nitesh V Chawla. 2022. Attre2vec: Unsupervised attributed edge representation learning. *Information Sciences* 592 (2022), 82–96.
- [3] Shaked Brody, Uri Alon, and Eran Yahav. 2022. How Attentive are Graph Attention Networks?. In *ICLR*. arXiv:2105.14491
- [4] Jiangxia Cao, Xixun Lin, Shu Guo, Luchen Liu, Tingwen Liu, and Bin Wang. 2021. Bipartite Graph Embedding via Mutual Information Maximization. In *Proceedings of the 14th ACM International Conference on Web Search and Data Mining (WSDM '21)*. Association for Computing Machinery, New York, NY, USA, 635–643. <https://doi.org/10.1145/3437963.3441783>
- [5] Rizal Fathony, Jenn Ng, and Jia Chen. 2023. Interaction-Focused Anomaly Detection on Bipartite Node-and-Edge-Attributed Graphs. In *2023 International Joint Conference on Neural Networks (IJCNN)*. IEEE, 1–10.
- [6] Zheng Gao, Gang Fu, Chungping Ouyang, Satoshi Tsutsui, Xiaozhong Liu, Jeremy Yang, Christopher Gessner, Brian Foote, David Wild, Ying Ding, et al. 2019. edge2vec: Representation learning using edge semantics for biomedical knowledge discovery. *BMC bioinformatics* 20, 1 (2019), 1–15.
- [7] Mathieu Garchery and Michael Granitzer. 2020. Adsage: Anomaly detection in sequences of attributed graph edges applied to insider threat detection at fine-grained level. *arXiv preprint arXiv:2007.06985* (2020).
- [8] Edward Giamphy, Jean-Loup Guillaume, Antoine Doucet, and Kevin Sanchis. 2023. A survey on bipartite graphs embedding. *Social Network Analysis and Mining* 13, 1 (2023), 54. <https://doi.org/10.1007/s13278-023-01058-z>
- [9] Gene H Golub and Charles F Van Loan. 1996. Matrix computations. *Johns Hopkins University Press, 3rd edition* (1996).
- [10] Liyu Gong and Qiang Cheng. 2019. Exploiting edge features for graph neural networks. In *Proceedings of the IEEE/CVF conference on computer vision and pattern recognition*. 9211–9219.
- [11] Aditya Grover and Jure Leskovec. 2016. Node2vec: Scalable feature learning for networks. *KDD 13-17-Augu* (2016), 855–864. arXiv:1607.00653
- [12] Nathan Halko, Per-Gunnar Martinsson, and Joel A Tropp. 2011. Finding structure with randomness: Probabilistic algorithms for constructing approximate matrix decompositions. *SIAM review* 53, 2 (2011), 217–288.
- [13] William L Hamilton, Rex Ying, and Jure Leskovec. 2017. Inductive representation learning on large graphs. In *NIPS*, Vol. 2017-December. 1025–1035. arXiv:1706.02216
- [14] William L Hamilton, Rex Ying, and Jure Leskovec. 2017. Representation learning on graphs: Methods and applications. *arXiv preprint arXiv:1709.05584* (2017).
- [15] Chaoyang He, Tian Xie, Yu Rong, Wenbing Huang, Junzhou Huang, Xiang Ren, Cyrus Shahabi, and Xi-Ang Ren. 2020. *Cascade-BGNN: Toward Efficient Self-supervised Representation Learning on Large-scale Bipartite Graphs*. Technical Report. <https://doi.org/10.1145/1122445.1122456> arXiv:1906.11994v3
- [16] Roger A Horn and Charles R Johnson. 2012. *Matrix analysis*. Cambridge university press.
- [17] Keke Huang, Jing Tang, Juncheng Liu, Renchi Yang, and Xiaokui Xiao. 2023. Node-wise diffusion for scalable graph learning. In *Proceedings of the ACM Web Conference 2023*. 1723–1733.
- [18] Wentao Huang, Yuchen Li, Yuan Fang, Ju Fan, and Hongxia Yang. 2020. BiANE: Bipartite Attributed Network Embedding. *SIGIR 2020 - Proceedings of the 43rd International ACM SIGIR Conference on Research and Development in Information Retrieval* 10, 20 (2020), 149–158. <https://doi.org/10.1145/3397271.3401068>
- [19] Jaehyeong Jo, Jinheon Baek, Seul Lee, Dongki Kim, Minki Kang, and Sung Ju Hwang. 2021. Edge representation learning with hypergraphs. *Advances in Neural Information Processing Systems* 34 (2021), 7534–7546.
- [20] Diederik P. Kingma and Jimmy Lei Ba. 2015. Adam: A method for stochastic optimization. In *arXiv Prepr. arXiv1412.6980*. arXiv. arXiv:1412.6980
- [21] Thomas N. Kipf and Max Welling. 2017. Semi-supervised classification with graph convolutional networks. *ICLR 2017* (sep 2017).
- [22] David A Levin and Yuval Peres. 2017. *Markov chains and mixing times*. Vol. 107. American Mathematical Soc.

- [23] Jiacheng Li, Jingbo Shang, and Julian McAuley. 2022. UCTopic: Unsupervised Contrastive Learning for Phrase Representations and Topic Mining. *Proceedings of the Annual Meeting of the Association for Computational Linguistics 1* (2022), 6159–6169. <https://doi.org/10.18653/v1/2022.acl-long.426> arXiv:2202.13469
- [24] Suxue Li, Haixia Zhang, Dalei Wu, Chuanting Zhang, and Dongfeng Yuan. 2018. Edge representation learning for community detection in large scale information networks. In *Mobility Analytics for Spatio-Temporal and Social Data: First International Workshop, MATES 2017, Munich, Germany, September 1, 2017, Revised Selected Papers 1*. Springer, 54–72.
- [25] Yiming Li, Siyue Xie, Xiaxin Liu, Qiu Fang Ying, Wing Cheong Lau, Dah Ming Chiu, Shou Zhi Chen, et al. 2021. Temporal graph representation learning for detecting anomalies in e-payment systems. In *2021 International Conference on Data Mining Workshops (ICDMW)*. IEEE, 983–990.
- [26] Yirui Liu, Xinghao Qiao, Liying Wang, and Jessica Lam. 2023. EEGNN: Edge Enhanced Graph Neural Network with a Bayesian Nonparametric Graph Model. In *International Conference on Artificial Intelligence and Statistics*. PMLR, 2132–2146.
- [27] Yao Ma, Xiaorui Liu, Tong Zhao, Yozen Liu, Jiliang Tang, and Neil Shah. 2021. A unified view on graph neural networks as graph signal denoising. In *Proceedings of the 30th ACM International Conference on Information & Knowledge Management*. 1202–1211.
- [28] Rajeev Motwani and Prabhakar Raghavan. 1995. *Randomized algorithms*. Cambridge university press.
- [29] Jianmo Ni, Jiacheng Li, and Julian McAuley. 2019. Justifying recommendations using distantly-labeled reviews and fine-grained aspects. *EMNLP-IJCNLP 2019 - 2019 Conference on Empirical Methods in Natural Language Processing and 9th International Joint Conference on Natural Language Processing, Proceedings of the Conference (2019)*, 188–197. <https://doi.org/10.18653/v1/d19-1018>
- [30] Mingdong Ou, Peng Cui, Jian Pei, Ziwei Zhang, and Wenwu Zhu. 2016. Asymmetric transitivity preserving graph embedding. *KDD 13-17-Aug* (2016), 1105–1114.
- [31] Bryan Perozzi, Rami Al-Rfou, and Steven Skiena. 2014. DeepWalk: Online learning of social representations. *SIGKDD (2014)*, 701–710. arXiv:1403.6652
- [32] Nils Reimers and Iryna Gurevych. 2020. Sentence-BERT: Sentence embeddings using siamese BERT-networks. *EMNLP-IJCNLP 2019 - 2019 Conference on Empirical Methods in Natural Language Processing and 9th International Joint Conference on Natural Language Processing, Proceedings of the Conference (2020)*, 3982–3992. <https://doi.org/10.18653/v1/d19-1410> arXiv:1908.10084
- [33] Arnab Sinha, Zhihong Shen, Yang Song, Hao Ma, Darrin Eide, Bo-june Paul Hsu, and Kuansan Wang. 2015. An overview of microsoft academic service (mas) and applications. In *WWW*. ACM, 243–246.
- [34] Gilbert Strang. 2022. *Introduction to linear algebra*. SIAM.
- [35] Guolei Sun and Xiangliang Zhang. 2019. A novel framework for node/edge attributed graph embedding. In *Advances in Knowledge Discovery and Data Mining: 23rd Pacific-Asia Conference, PAKDD 2019, Macau, China, April 14-17, 2019, Proceedings, Part III 23*. Springer, 169–182.
- [36] Jian Tang, Meng Qu, Mingzhe Wang, Ming Zhang, Jun Yan, and Qiaozhu Mei. 2015. LINE: Large-scale information network embedding. *WWW 2015 (2015)*, 1067–1077. arXiv:1503.03578
- [37] Jie Tang, Duo Zhang, and Limin Yao. 2007. Social Network Extraction of Academic Researchers. In *ICDM'07*. 292–301.
- [38] Jie Tang, Jing Zhang, Limin Yao, Juanzi Li, Li Zhang, and Zhong Su. 2008. ArnetMiner: Extraction and mining of academic social networks. *SIGKDD (2008)*, 990–998.
- [39] Petar Veličković, Guillem Cucurull, Arantxa Casanova, Adriana Romero, Pietro Liò, and Yoshua Bengio. 2017. Graph Attention Networks. In *ICLR 2018*.
- [40] Petar Veličković, William Fedus, William L Hamilton, Pietro Liò, Yoshua Bengio, and R Devon Hjelm. 2018. Deep Graph Infomax. In *ICLR*.
- [41] Andrew Z Wang, Rex Ying, Pan Li, Nikhil Rao, Karthik Subbian, and Jure Leskovec. 2021. Bipartite dynamic representations for abuse detection. In *Proceedings of the 27th ACM SIGKDD Conference on Knowledge Discovery & Data Mining*. 3638–3648.
- [42] Hewen Wang, Renchi Yang, Keke Huang, and Xiaokui Xiao. 2023. Efficient and Effective Edge-wise Graph Representation Learning. In *Proceedings of the 29th ACM SIGKDD Conference on Knowledge Discovery and Data Mining*. 2326–2336.
- [43] Hewen Wang, Renchi Yang, and Jieming Shi. 2023. Anomaly Detection in Financial Transactions Via Graph-Based Feature Aggregations. In *Big Data Analytics and Knowledge Discovery: 25th International Conference, DaWaK 2023, Penang, Malaysia, August 28–30, 2023, Proceedings*. Springer-Verlag, Berlin, Heidelberg, 64–79. https://doi.org/10.1007/978-3-031-39831-5_6
- [44] Jianian Wang, Sheng Zhang, Yanghua Xiao, and Rui Song. 2022. A Review on Graph Neural Network Methods in Financial Applications. *Journal of Data Science* 20, 2 (2022), 111–134.
- [45] Ziming Wang, Jun Chen, and Haopeng Chen. 2021. EGAT: Edge-featured graph attention network. In *Artificial Neural Networks and Machine Learning-ICANN 2021: 30th International Conference on Artificial Neural Networks, Bratislava, Slovakia, September 14–17, 2021, Proceedings, Part 1 30*. Springer, 253–264.
- [46] Felix Wu, Tianyi Zhang, Amauri Holanda de Souza, Christopher Fifty, Tao Yu, and Kilian Q. Weinberger. 2019. Simplifying graph convolutional networks. In *arXiv*.
- [47] Xueyi Wu, Yuanyuan Xu, Wenjie Zhang, and Ying Zhang. 2023. Billion-Scale Bipartite Graph Embedding: A Global-Local Induced Approach. *Proc. VLDB Endow.* 17, 2 (2023), 175–183. <https://doi.org/10.14778/3626292.3626300>
- [48] Yulin Wu, Xiangting Hou, Wen Jun Tan, Zengxiang Li, and Wentong Cai. 2017. Efficient parallel simulation over social contact network with skewed degree distribution. In *Proceedings of the 2017 ACM SIGSIM Conference on Principles of Advanced Discrete Simulation*. 65–75.
- [49] Zhanghao Wu, Paras Jain, Matthew Wright, Azalia Mirhoseini, Joseph E Gonzalez, and Ion Stoica. 2021. Representing long-range context for graph neural networks with global attention. *Advances in Neural Information Processing Systems* 34 (2021), 13266–13279.
- [50] Hansheng Xue, Luwei Yang, Vaibhav Rajan, Wen Jiang, Yi Wei, and Yu Lin. 2021. Multiplex Bipartite Network Embedding Using Dual Hypergraph Convolutional Networks. In *Proceedings of the Web Conference 2021 (WWW '21)*. Association for Computing Machinery, New York, NY, USA, 1649–1660. <https://doi.org/10.1145/3442381.3449954>
- [51] An Yan, Zhankui He, Jiacheng Li, Tianyang Zhang, and Julian McAuley. 2023. Personalized Showcases: Generating Multi-Modal Explanations for Recommendations. *SIGIR 2023 - Proceedings of the 46th International ACM SIGIR Conference on Research and Development in Information Retrieval* 5, 23 (2023), 2251–2255. <https://doi.org/10.1145/3539618.3592036> arXiv:2207.00422
- [52] Hongqiang Yan, Yan Jiang, and Guannan Liu. 2018. Telecom fraud detection via attributed bipartite network. In *2018 15th International Conference on Service Systems and Service Management (ICSSSM)*. IEEE, 1–6.
- [53] Liang Yang, Chuan Wang, Junhua Gu, Xiaochun Cao, and Bingxin Niu. 2021. Why do attributes propagate in graph convolutional neural networks?. In *Proceedings of the AAAI Conference on Artificial Intelligence*, Vol. 35. 4590–4598.
- [54] Renchi Yang. 2022. Efficient and Effective Similarity Search over Bipartite Graphs. In *Proceedings of the ACM Web Conference 2022*. 308–318.
- [55] Renchi Yang and Jieming Shi. 2024. Efficient High-Quality Clustering for Large Bipartite Graphs. *Proceedings of the ACM on Management of Data* 2, 1 (2024), 1–27.
- [56] Renchi Yang, Jieming Shi, Keke Huang, and Xiaokui Xiao. 2022. Scalable and Effective Bipartite Network Embedding. In *Proceedings of the 2022 International Conference on Management of Data*. 1977–1991.
- [57] Renchi Yang, Jieming Shi, Xiaokui Xiao, Yin Yang, and Sourav S. Bhowmick. 2020. Homogeneous network embedding for massive graphs via reweighted personalized pagerank. *VLDB* 13, 5 (2020), 670–683. arXiv:1906.06826
- [58] Renchi Yang, Jieming Shi, Xiaokui Xiao, Yin Yang, Juncheng Liu, and Sourav S. Bhowmick. 2020. Scaling attributed network embedding to massive graphs. *VLDB* 14, 1 (2020), 37–49. arXiv:2009.00826
- [59] Renchi Yang, Jieming Shi, Yin Yang, Keke Huang, Shiqi Zhang, and Xiaokui Xiao. 2021. Effective and scalable clustering on massive attributed graphs. In *Proceedings of the Web Conference 2021*. 3675–3687.
- [60] Wei Yu, Wenkai Wang, Guangquan Xu, Huaming Wu, Hongyan Li, Jun Wang, Xiaoming Li, and Juan Liu. 2023. MRFS: Mining Rating Fraud Subgraph in Bipartite Graph for Users and Products. *IEEE Transactions on Computational Social Systems* (2023).
- [61] Jie Zhang, Yuxiao Dong, Yan Wang, Jie Tang, and Ming Ding. 2019. Prone: Fast and scalable network representation learning. In *IJCAI*. 4278–4284.
- [62] Yao Zhang, Yun Xiong, Xiangnan Kong, and Yangyong Zhu. 2017. Learning node embeddings in interaction graphs. In *Proceedings of the 2017 ACM on Conference on Information and Knowledge Management*. 397–406.
- [63] Ziwei Zhang, Jian Pei, Peng Cui, Xuanrong Yao, Xiao Wang, and Wenwu Zhu. 2018. Arbitrary-order proximity preserved network embedding. *KDD (2018)*, 2778–2786.
- [64] Tao Zhou, Jie Ren, Matúš Medo, and Yi-Cheng Zhang. 2007. Bipartite network projection and personal recommendation. *Physical review E* 76, 4 (2007), 046115.
- [65] Yuchen Zhou, Hongtao Huo, Zhiwen Hou, Lingbin Bu, Jingyi Mao, Yifan Wang, Xiaojun Lv, and Fanliang Bu. 2023. Co-embedding of edges and nodes with deep graph convolutional neural networks. *Scientific Reports* 13, 1 (2023), 16966.
- [66] Meiqi Zhu, Xiao Wang, Chuan Shi, Houye Ji, and Peng Cui. 2021. Interpreting and unifying graph neural networks with an optimization framework. In *Proceedings of the Web Conference 2021*. 1215–1226.